Pressure-induced flat bands in one-dimensional moiré superlattices of collapsed chiral carbon nanotubes

Xianliang Zhou,[1,2,*] Yi Chen,[1,2] Jiajun Chen,[1,2] Cheng Hu,[1,2] Bosai Lyu,[1,2] Kunqi Xu,[1,2] Shuo Lou,[1,2] Peiyue Shen,[1,2] Saiqun Ma,[1,2] Zhenghan Wu,[1,2] Yufeng Xie,[1,2] Zhichun Zhang,[1,2] Zhiguo Lü,[1,2] Weidong Luo,[1,2,3] Qi Liang,[1,2,4] Lede Xian,[5,6,†] Guangyu Zhang,[5,7,8] and Zhiwen Shi[1,2,4,‡]

[1]*Key Laboratory of Artificial Structures and Quantum Control (Ministry of Education), Shenyang National Laboratory for Materials Science, School of Physics and Astronomy, Shanghai Jiao Tong University, Shanghai 200240, China*

[2]*Collaborative Innovation Center of Advanced Microstructures, Nanjing University, Nanjing 210093, China*

[3]*Institute of Natural Sciences, Shanghai Jiao Tong University, Shanghai 200240, China*

[4]*Tsung-Dao Lee Institute, Shanghai Jiao Tong University, Shanghai 200240, China*

[5]*Songshan Lake Materials Laboratory, Dongguan, Guangdong 523808, China*

[6]*Max Planck Institute for the Structure and Dynamics of Matter, Center for Free Electron Laser Science, 22761 Hamburg, Germany*

[7]*Beijing National Laboratory for Condensed Matter Physics and Institute of Physics, Chinese Academy of Sciences, Beijing 100190, China*

[8]*School of Physical Sciences, University of Chinese Academy of Sciences, Beijing 100190, China*

(Received 20 September 2023; revised 2 November 2023; accepted 4 December 2023; published 2 January 2024)

Two-dimensional (2D) moiré superlattices have been extensively investigated, whereas the one-dimensional (1D) moiré superlattices have remained largely unexplored, due to the difficulty in achieving 1D moiré superlattices experimentally. Recent theoretical studies have predicted that certain collapsed chiral carbon nanotubes (CNTs) behave as 1D moiré superlattices with novel strongly correlated physics, owing to the emergence of 1D flat bands. However, the realization of 1D flat bands is limited to CNTs with a narrow range of chirality, which hinders the experimental investigation. Here, using molecular dynamics simulations and tight-binding calculations, we reveal that the application of external pressure can induce 1D moiré flat bands in a wide range of collapsed CNTs of both metallic and semiconducting types. We further provide a comprehensive analysis of the emergence of the 1D flat bands, and derive critical pressures for CNTs of various chiralities. Our study presents a versatile approach for creating 1D flat bands, and therefore could greatly facilitate the experimental exploration of 1D strongly correlated physics in collapsed CNT moiré superlattices.

DOI: 10.1103/PhysRevB.109.045105

I. INTRODUCTION

Two-dimensional (2D) moiré superlattices have attracted tremendous research interest [1–8] since the discovery of superconducting [9] and correlated-insulating [10] behavior in magic-angle twisted bilayer graphene. At the magic angle, the Fermi velocity in graphene drops to near zero and moiré flat bands emerge due to the modulation from long-range superlattice potential [11–15]. Consequently, the Coulomb interaction becomes dominant over the kinetic energy, leading to strongly correlated states. On the other hand, the Coulomb interaction effect is known to be enhanced in lower-dimensional materials due to the reduced degree of freedom in space and the reduced electrostatic screening. For example, novel correlating Luttinger-liquid behavior was predicted [16,17] in carbon nanotubes (CNTs) and has been experimentally observed [18–20]. Therefore, one-dimensional (1D) moiré superlattices provide an appealing platform for studying strongly correlated physics [21]. Recently, a few 1D moiré systems have been studied including incommensurate double-walled CNTs [22], CNTs on hexagonal boron nitride [23–25] and collapsed chiral CNTs [26–28].

Recent theoretical studies have predicted that collapsed chiral CNTs behave as 1D moiré superlattices with novel strongly correlated physics, owing to the emergence of 1D flat bands [26,27]. In such systems, it is estimated that the Coulomb interaction is much larger than the kinetic energy due to the extreme flatness (< 1 meV) of the band structure. However, the realization of 1D flat bands is limited to CNTs with a narrow range of chirality, which strongly hinders the experimental investigation due to the lack of methods for growing CNTs with specific chirality in experiment. On the other hand, pressure can alter the physical and chemical properties of materials [28–30], making it a versatile tool in material research of moiré physics [31–33]. Theoretical and experimental findings have demonstrated that applying external pressure to 2D twisted bilayer graphene can induce strongly correlated behavior [5,8], even at twist angles other than the magic angle.

In this paper, we demonstrate that the application of external pressure can induce strongly correlated behavior in a wide range of collapsed chiral CNTs, as identified by the presence of flat bands. This is achieved through the use of molecular

*fishballien@sjtu.edu.cn
†xianlede@sslab.org.cn
‡zwshi@sjtu.edu.cn

dynamics simulations and tight-binding calculations. We find that both the bandwidth and the bandgap can be tuned in both metallic and semiconducting collapsed CNTs by simply applying external pressure. We further provide a comprehensive analysis of the emergence of 1D flat bands and critical pressures for various collapsed CNTs. Our study presents an approach to create the 1D flat bands, which could significantly reduce the difficulty in experimental observations of 1D strongly correlated physics in collapsed CNT moiré superlattices.

II. METHODS

A. Geometry

Carbon nanotubes (CNTs) are characterized by their chiral indices (n, m), which are associated with the chiral vector $\mathbf{C} = n\mathbf{a}_1 + m\mathbf{a}_2$, where $\mathbf{a}_1$ and $\mathbf{a}_2$ represent the two primitive vectors in graphene. The chiral angle θ of a CNT represents the relative angle between the chiral vector $\mathbf{C}$ and the zigzag direction, which can be easily related to the chiral indices (n, m) [34]. When the diameter of the CNT is larger than approximate 4 nm, the elastic energy of the tube may not be sufficient to maintain its cylindrical shape, causing it to spontaneously collapse into a flat shape [35–37].

Chiral CNTs are nanotubes that lack inversion symmetry, characterized by nonzero chiral indices (n, m), where $n \neq m$, and correspondingly the chiral angle θ in chiral CNTs is nonzero. Due to the nonzero θ, the two halves of the chiral CNT unit cell misalign when collapsed, and result in the presence of 1D moiré superlattice in collapsed chiral CNTs [26] as shown in Fig. 1. The moiré twist angle θ_M in a collapsed chiral CNT is defined as the relative angle between upper and lower layers, which is twice as the chiral angle θ of the CNT, i.e., $\theta_M = 2\theta$. Recent studies show that the flat bands in collapsed chiral CNTs are spatially localized in the AA stacking region [26,27], so in order to obtain full moiré islands with AA stacking in collapsed chiral CNT, the chiral vector $\mathbf{C}$ must pass through at least one carbon atom of the graphene lattice [26]. The simplest possible structures are $(2m, 2)$ CNTs with C_2 symmetry [26] or $(3m, 3)$ with C_3 symmetry [27]. In this paper, we investigate both metallic and semiconducting chiral CNTs with focused chiral indices $(2m, 2)$; however, our findings can be extended to CNTs with other indices or symmetries.

B. Molecular dynamics simulations

Molecular dynamics calculations are used to simulate the collapsed chiral CNTs. The large-scale atomic/molecular massively parallel simulator (LAMMPS) package [38] is used to obtain reliable structures of collapsed CNTs without and with external pressure. The interaction between carbon atoms is computed using the adaptive intermolecular reactive empirical bond order (AIREBO) [39] potential. The system is subjected to periodic conditions with sufficiently large supercells to prevent spurious interactions between CNT replicas and the time step of the simulation is 1 fs.

To obtain the structure of spontaneously collapsed CNTs without external pressure, we adopt the strategy in previous study [26]. First, the cylindrical CNT is collapsed by applying a external force (2 eV/Å) on one side of the tube. Then the external force is removed and the system is relaxed using a conjugate gradient algorithm until all forces are below 10^{-8} eV/Å. CNTs with a sufficient diameter remain in a collapsed structure due to interlayer van der Waals attraction. Figure 1 shows an example of the converged final geometry of a collapsed CNT. In the case of a collapsed CNT subjected to external pressure, two auxiliary graphene layers are fixed on both sides of the spontaneously collapsed CNT, and only the coordinates of CNT in between are relaxed. The application of external pressure induces mainly vertical compression of collapsed CNT resulting in a decrease of interlayer distance d (Fig. 2), and the compression strain defined in this paper is $\varepsilon = (d - d_0)/d_0$, where d_0 represents the interlayer distance at zero pressure (Fig. 1). Different fixed distances between two graphene layers correspond to different compression or different pressure applied on the collapsed CNT, and the pressure values are further determined from the output force data in LAMMPS.

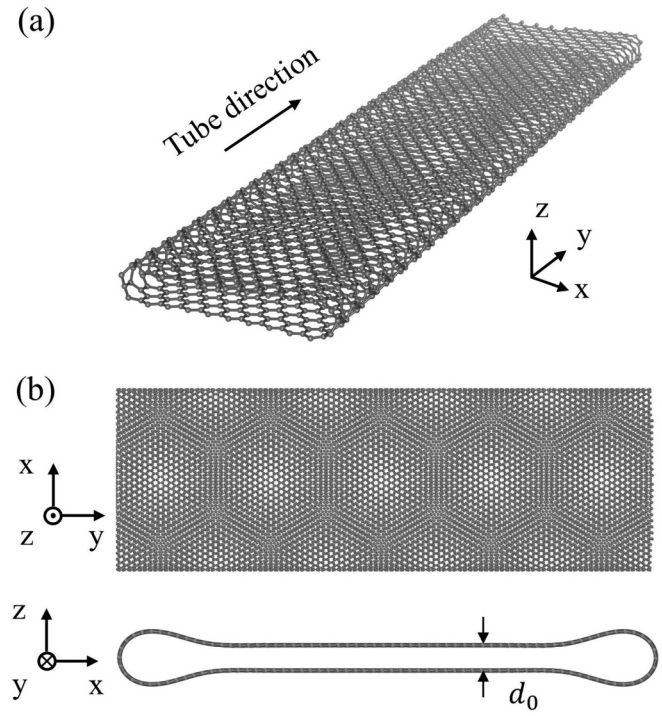

FIG. 1. (a) A schematic representation of a collapsed chiral carbon nanotube. (b) Top and side views of the collapsed chiral CNT, illustrating the 1D moiré pattern formed by two misaligned layers of the collapsed chiral CNT.

C. Tight-binding model

Due to the large number of atoms in the collapsed CNT systems, the tight-binding model is appropriate to calculate the band structure of the system. The LAMMPS relaxed structure of the collapsed CNT is used as the input for the tight-binding model, considering the carbon p_z orbitals. The tight-binding Hamiltonian is written as

$$H = -\sum_{i,j} t(\mathbf{R}_i - \mathbf{R}_j)|\mathbf{R}_i\rangle\langle\mathbf{R}_j| + \text{H.c.}, \tag{1}$$

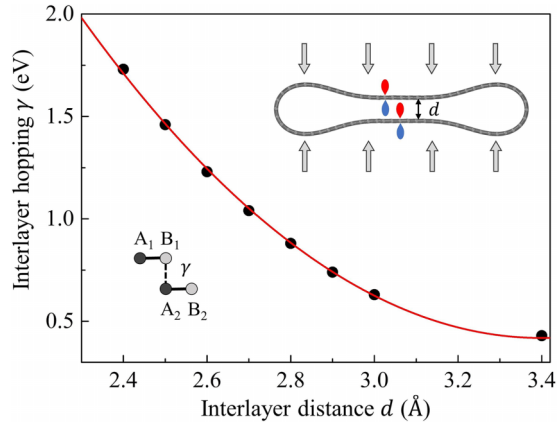

FIG. 2. Interlayer distance d dependence of the interlayer hopping parameter γ from the density functional theory result [41]. The quadratic fit for γ is given by the red line. Upper inset shows a schematic representation of a collapsed chiral CNT under pressure and the p_z atomic orbitals of carbon atoms, with the colors indicating different signs. Vertical compression leads to a decrease in interlayer distance and an increase in interlayer coupling. Lower inset shows a schematic representation of interlayer hopping parameter γ.

where $\mathbf{R}_i$ and $|\mathbf{R}_i\rangle$ represent the position and atomic state at site i, and $t(\mathbf{R}_i - \mathbf{R}_j)$ is the hopping energy between the sites i and j. The pressure-modified Slater-Koster-type hopping function [26,40] is employed for the flat collapsed part of the CNT as

$$-t(\mathbf{R}) = V(R)\left[1 - \left(\frac{\mathbf{R}\cdot\mathbf{e}_z}{R}\right)^2\right] + \gamma(R)\left(\frac{\mathbf{R}\cdot\mathbf{e}_z}{R}\right)^2, \quad (2)$$

where the hopping parameters are

$$V(R) = V^0_{pp\pi}\exp\left(-\frac{R-a_0}{r_0}\right), \quad (3)$$

and

$$\gamma(R) = \begin{cases} V^0_{pp\sigma}\exp\left(-\frac{R-d_0}{r_0}\right) & R > d_0 \\ \gamma_2\left(\frac{R-d_0}{d_0}\right)^2 + \gamma_1\left(\frac{R-d_0}{d_0}\right) + \gamma_0 & R < d_0 \end{cases}, \quad (4)$$

where $\mathbf{e}_z$ is the unit vector perpendicular to the collapsed plane of the CNT, $a_0 = 1.42$ Å is the distance of neighboring carbon atoms, $d_0 = 3.4$ Å is the interlayer distance, $V^0_{pp\pi} = -2.7$ eV is the in-plane nearest-neighbor coupling, $V^0_{pp\sigma} = 0.42$ eV is the interlayer coupling between two orbitals in AB stacking and $r_0 = 0.319a_0$ is the exponential decay length of the coupling [40]. Previous studies have shown that compression perpendicular to the plane has a negligible effect on the in-plane tight-binding parameters, but significantly enhances the interlayer hopping energy [8]. Consequently, when the external pressure is applied, we adopt the same in-plane hopping function $V(R)$ as the zero-pressure case in Eq. (3), while the interlayer hopping function $\gamma(R)$ is adjusted as a quadratic fit to the density functional theory result of AB stacked bilayer graphene [8,41] in Eq. (4) as shown in Fig. 2 with $\gamma_2 = 14.93$ eV, $\gamma_1 = 0$, and $\gamma_0 = 0.42$ eV. It should be noted that the interlayer hopping $\gamma(R)$ arises from the direct overlap of carbon atoms and shows only a slight dependence on the stacking order. Therefore, using results of AB stacked bilayer graphene to fit the pressure dependence of interlayer hopping can well describe the collapsed CNT moiré superlattice under pressure. Only the $V(R)$ hopping term that depends on the relevant distance between carbon atoms is taken into account for the outer lobes of the collapsed CNT, which is a good approximation to the collapsed CNT system [26].

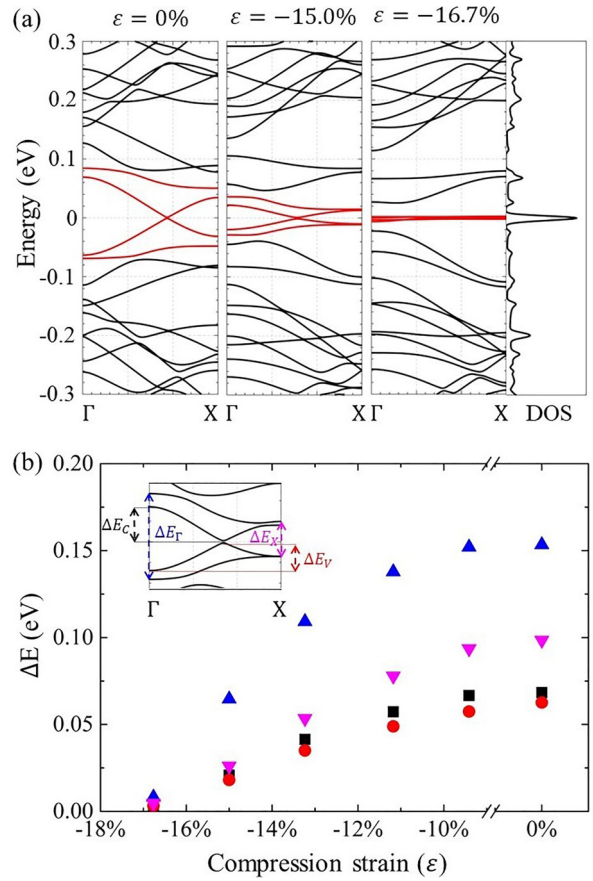

FIG. 3. (a) Evolution of band structure of the collapsed metallic (98, 2) CNT under external compression with four central bands highlighted in red. The density of states at $\varepsilon = -16.7\%$ is shown on the right panel in (a). (b) Energy span and bandwidth of the collapsed metallic (98, 2) CNT as a function of the compression strain. The energy span of the central four bands at Γ and X are ΔE_Γ and ΔE_X, and the bandwidth of the lowest conduction band and the highest valence band are ΔE_C and ΔE_V. Inset schematically represents these four quantities. Notably, at a critical compression of $\varepsilon = -16.7\%$, all the four quantities drop to near zero.

III. RESULTS AND DISCUSSION

A. Pressure-induced flat bands in collapsed metallic CNTs

Figure 3 presents the pressure-induced flat bands in the collapsed metallic (98, 2) CNT. Due to its large diameter (∼7.75 nm), the (98, 2) CNT collapses spontaneously to a flat shape forming a 1D moiré superlattice, with an interlayer distance $d_0 = 3.4$ Å after structure relaxation in molecular dynamics simulations. Figure 3(a) shows the evolution of band structure for the collapsed metallic (98, 2) CNT under external pressure. The Fermi level is set at zero in this paper. The band structure at $\varepsilon = 0$ represents to the spontaneously

collapsed CNT and has a Dirac cone at the Fermi level indicating metallic behavior as shown in Fig. 3(a). The collapsed CNT shows reduced band velocities at high-symmetry points compared to the uncollapsed CNT due to the interlayer coupling, which is consistent with previous study [26]. As the external pressure increases, the interlayer distance d decreases (i.e., compression strain ε increases). It is evident that the central four bands highlighted in red in Fig. 3(a) significantly shrink, and at a critical compression $\varepsilon = -16.7\%$ these four bands become remarkably flat, with a rather small bandwidth <4 meV. The rightmost panel in Fig. 3(a) displays the density of states at $\varepsilon = -16.7\%$. A prominent peak single out at the Fermi level from the rest of the spectrum, corresponding to four isolated flat bands in compressed (98, 2) CNT. In contrast to CNTs with a larger diameter, where eight flat bands emerge under the magic-angle condition [26], only four bands become pressure-induced flat. The other four bands are gapped from the central four bands with an energy gap $\sim$20 meV, and remain dispersive.

To quantitatively asses the flatness of the band structure, we define the bandwidth of conduction band ΔE_C and valence band ΔE_V, as well as the energy span, the difference between the maximum and minimum energies of central four bands at two high-symmetry points ΔE_Γ and ΔE_X [schematically represented in the inset of Fig. 3(b)]. These four quantities represent the kinetic energy of the bands, and are the relevant quantities for estimating the importance of Coulomb interaction in the system [26]. Figure 3(b) shows the evolution of these four quantities as increased compression. The band structure of collapsed (98, 2) CNT remains almost unchanged until the compression reaches $\varepsilon \approx -10\%$. After this point, both the bandwidth and energy span of the central four bands decrease monotonically. At the critical compression, $\varepsilon = -16.7\%$, both bandwidth and energy span decrease to nearly zero ($\Delta E_\Gamma = 8.2$ meV, $\Delta E_X = 4.7$ meV, $\Delta E_C = 2.1$ meV, and $\Delta E_V = 3.2$ meV), indicating the emergence of pressure-induced flat bands in the collapsed (98, 2) CNT.

Another collapsed metallic CNT with chirality of (62, 2) is also studied (see the Supplemental Material [42]). For the (62, 2) CNT, at a critical compression $\varepsilon = -24.3\%$, four moiré flat bands emerge. More detailed results can be found in the Supplemental Material [42].

B. Pressure-induced flat bands in collapsed semiconducting CNTs

Figure 4 presents the pressure-induced flat bands in the collapsed semiconducting (94, 2) CNT. Similar to (98, 2) CNT, the (94, 2) CNT also has a large diameter ($\sim$7.44 nm) and collapse spontaneously to a flat shape forming a 1D moiré superlattice with an interlayer distance $d_0 = 3.4$ Å. Figure 4(a) shows the evolution of band structure for the collapsed semiconducting (94, 2) CNT under external pressure. The collapsed semiconducting CNT exhibits an intrinsic bandgap $\sim$40 meV as shown in Fig. 4(a) at $\varepsilon = 0$. As the external pressure increases, the bandgap at the Fermi level decreases accordingly, changing from a semiconducting behavior at $\varepsilon = 0$ to a semimetallic behavior at the critical compression $\varepsilon = -17.4\%$ with a minimal bandgap < 1 meV. The central twelve flat bands with bandwidth $\sim$10 meV are

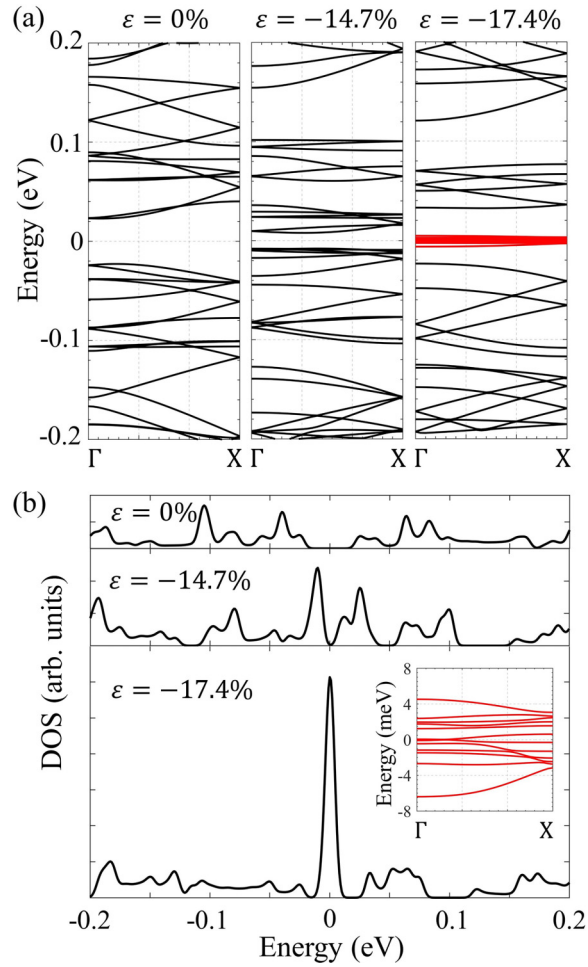

FIG. 4. Evolution of (a) band structure and (b) density of states for the collapsed semiconducting (94, 2) CNT under external compression with twelve central flat bands highlighted in red. Inset in (b) represent the detailed zoom-in band structure at $\varepsilon = -17.4\%$.

highlighted in red in Fig. 4(a) at $\varepsilon = -17.4\%$ and are zoomed in as shown in the inset of Fig. 4(b). In the collapsed semiconducting CNT, twelve flat bands emerge under critical pressure whereas only four flat bands emerge in the collapsed metallic CNT. The different numbers of emerged flat bands arise from band folding of CNTs. In the collapsed metallic (98, 2) CNT, the translational lattice parameter along the CNT is $\sim$7 nm containing one full AA stacking moiré area per unit cell. In contrast in the collapsed semiconducting (94, 2) CNT, the translational lattice parameter is $\sim$20 nm, three times larger than that of the metallic CNT, and contains three full AA stacking moiré areas per unit cell [27]. As a result, the Brillouin zone in semiconducting (94, 2) CNT is three times folded compared with the metallic (98, 2) CNT, which explains the different numbers of flat bands emerged in the two cases.

Figure 4(b) shows the evolution of density of states. The peaks in the density of states correspond to the band edge. It can be observed that the peaks near the Fermi level gradually come closer together with increased compression strain and merge into one peak, which corresponds to a semiconductor-metal transition. When compression strain

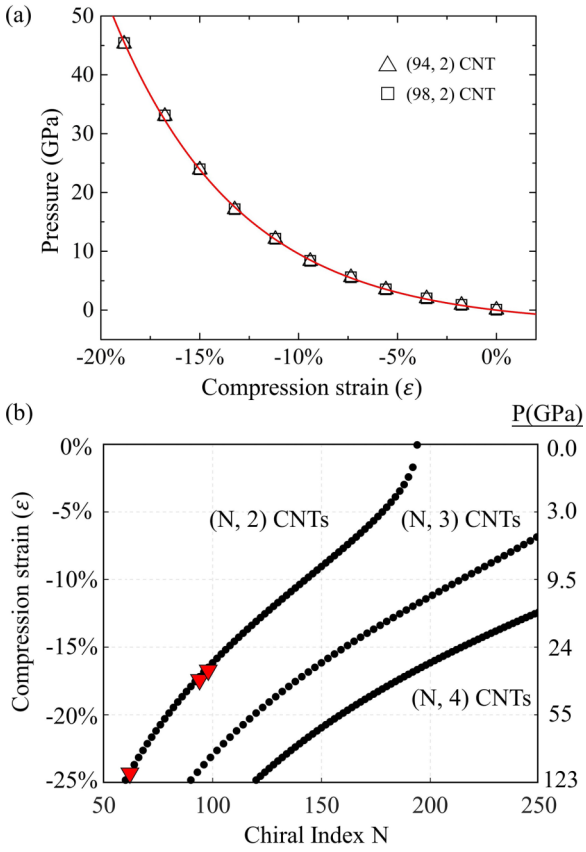

FIG. 5. (a) The calculated required external pressure as a function of compression strain ε for (94, 2) and (98, 2) collapsed CNTs, represented by triangles and squares respectively, and with an exponential fit (red line) given in the text. The fitting line is expected to applicable to CNTs of other chiralities. (b) The critical-compression and critical-pressure dependence curve on the chiral index for various CNTs. The three red triangles denoted the three collapsed CNTs studied in this paper.

reaches to the critical value $\varepsilon = -17.4\%$, a prominent peak isolated from the rest of the spectrum emerges at Fermi level indicating the emergence of pressure-induced flat bands. The bandgap between the central twelve flat bands and the rest of spectrum is approximately 20 meV.

C. Pressure-compression relation in collapsed CNTs

Above sections have discussed the critical compressions for semiconducting (94, 2) and metallic (98, 2) collapsed CNTs. However, direct tuning of compression in experimental is difficult. A feasible way to tune the compression is through applying external pressure, which can be easily adjusted experimentally. Therefore, it is useful for experimentalists to work out the relation between the compression strain and the pressure. Figure 5(a) presents the calculated external pressure P as a function of compression strain ε for semiconducting (94, 2) and metallic (98, 2) collapsed CNTs using the molecular dynamics simulation. The pressure P for both collapsed CNTs are almost identical under different compression conditions, and can be accurately described by the exponential function form

$$P = A(e^{-B\varepsilon} - 1), \tag{5}$$

with $A = 2.53$ GPa and $B = 15.64$ shown as a fitted red line in Fig. 5(a). Combining with Figs. 3 and 4, it is found that flat bands emerge at $P \approx 35.9$ GPa for the collapsed (94, 2) CNT and $P \approx 31.9$ GPa for the collapsed (98, 2) CNT. Moreover, the similar fitted curves observed for both collapsed (94, 2) and (98, 2) in Fig. 5(a) indicate that the pressure-compression relationship of collapsed CNTs is independent of the CNT chirality.

D. Critical pressure for CNTs with various chiralities

In order to provide more valuable information for experimentalists, we derived and computed the critical pressure of flat bands for CNTs with various chiralities, including $(N, 2)$, $(N, 3)$, and $(N, 4)$ series.

Similar to the case in 2D twisted-bilayer graphene system [5,8], in the 1D collapsed CNT system, the emergence of flat bands can be qualitatively understood by considering the competition between the kinetic energy E_k and interlayer coupling γ in the upper and lower layers. The kinetic energy of Bloch states in each layer of collapsed CNT is approximately $E_k \sim \pm\hbar v_F G\theta_M/2$, where $\hbar$ is the reduced Plank constant, v_F is the Fermi velocity of monolayer graphene, G is the magnitude of the wavevector $\Gamma - K$ in graphene, and θ_M is the moiré twist angle between upper and lower layer in the collapsed chiral CNT. When the interlayer hopping energy γ is equal to the magnitude of kinetic energy E_k in each layer, near zero eigenvalues and hence flat bands are expected [8,10,14].

Without external pressure, the flat bands emerge in 1D moiré superlattice of collapsed CNT at a moiré twist angle $\theta_0 \approx 1.1^\circ$ (the so-called magic angle), which corresponds to a chiral CNT with chirality of (176, 2) [26]. If external pressure is applied to the collapsed CNT, the interlayer hopping γ increases (Fig. 2), resulting in a proportional increase in the critical angle θ_c at which flat bands emerge. For example, as shown in Fig. 2, at $\varepsilon = -16.7\%$ ($d \approx 2.83$ Å) the interlayer hopping γ is nearly doubled $\gamma \approx 2\gamma_0$, and flat bands also emerge at a nearly doubled moiré twist angle of approximately 2.2° in the collapsed CNT with chirality of (98, 2) as shown in Fig. 3.

Using our previous quadratic dependence assumption of interlayer hopping strength on compression [Eq. (4)], and make the substitution $(\hbar v_F G)/2 \to \gamma_0/\theta_0$, we can obtain an expression of the critical compression $\varepsilon_c(\theta_M)$ for collapsed CNTs with the moiré twist angle θ_M, which is similar to the 2D case [8] as

$$\left(\frac{\gamma_2}{\gamma_0}\right)\varepsilon_c(\theta_M)^2 + \left(\frac{\gamma_1}{\gamma_0}\right)\varepsilon_c(\theta_M) + 1 = \frac{\theta_M}{\theta_0}. \tag{6}$$

Through Eqs. (5) and (6), we can get a critical pressure $P_c(\theta_M)$ relation for collapsed CNTs, at which flat bands emerge in a collapsed CNT with a moiré twist angle θ_M. Considering that the moiré twist angle is twice as the chiral angle in CNTs, i.e., $\theta_M = 2\theta$, we can finally obtain the critical-pressure relation with the chiral index N of various collapsed CNTs (see Supplemental Material [42]) as shown in Fig. 5(b). Three

collapsed CNTs calculated in this paper are denoted as red triangle in Fig. 5(b). In Fig. 5(b), the moiré twist angle at zero pressure θ_0 is used as a fitting parameter to fit the three data in this paper, and the fitted value is $\theta_0 \approx 1.02^\circ$, which is very close to the value in the previous study [26] $\theta_0 \approx 1.1^\circ$.

The Coulomb interaction U in the collapsed CNT systems can be estimated using the formula $U = \frac{e^2}{4\pi\epsilon d}$, where e is the electron charge, ϵ is the effective dielectric constant, and d is the effective linear dimension. The typical value for the effective dielectric constant ϵ is approximately 10. The effective linear dimension d in the collapsed CNT system is the unit-cell length along the CNT tube direction $\sim$7 nm. Combining these two values, we can obtain that the Coulomb interaction U is approximately 20 meV in the collapsed CNT systems under external pressure. This value exceeds both the bandwidth of the central flat bands and the bandgap between the flat and remote nonflat bands, and the correlated charge transfer insulator scenario may appear at the half-filling of the flat bands [43–45]. Therefore, we conclude that the collapsed chiral CNTs systems under external pressure exhibit 1D strongly correlated behavior. Figure 5(b) provides an experimental guidance for observing 1D strongly correlated physics in 1D moiré superlattice of collapsed chiral CNTs.

IV. CONCLUSIONS

In conclusion, we have demonstrated that the application of external pressure can alter the band structure of 1D moiré superlattices of collapsed chiral CNTs. Specifically, both the bandwidth and the bandgap in collapsed CNTs can be changed by the applied external pressure. At the critical pressure, 1D flat bands emerge, indicating the presence of strongly correlated phenomena. Four (twelve) flat bands as well as a prominent peak in density of states single out from the rest of the spectrum, with a bandgap $\sim$20 meV in the metallic (semiconducting) collapsed CNT. Moreover, the application of pressure can induce 1D flat bands in collapsed CNTs with a wide range of chiralities, which significantly reduces the difficulty in experimental realization of 1D strongly correlated physics. We further provide a comprehensive analysis of the emergence of 1D flat bands, and derive the critical-pressure relation for various collapsed CNTs. Our study provides an experimental guidance to create 1D flat bands and an approach to control strongly correlated phenomena in 1D moiré superlattice systems.

ACKNOWLEDGMENTS

This work is supported by the open research fund of Songshan Lake Materials Laboratory (Grant No. 2021SLABFK07), the National Key R&D Program of China (Grant No. 2021YFA1202902), and the National Natural Science Foundation of China (Grants No. 12374292, No. 12074244, and No. 11774226). K.X. acknowledges support from the China Postdoctoral Science Foundation (Grant No. 2022M712087). L.X. acknowledges the support by the National Key Research and Development Program of China (Grant No. 2022YFA1403501), the Key-Area Research and Development Program of Guangdong Province of China (Grant No. 2020B0101340001), the Hefei National Research Center for Physical Sciences at the Microscale (Grant No. KF2021003) and the MPI partner group between Songshan Lake Materials Laboratory and Max Planck Institute for the Structure and Dynamics of Matter. The computations in this paper were run on the π 2.0 cluster supported by the Center for High Performance Computing at Shanghai Jiao Tong University.

[1] G. Chen, A. L. Sharpe, P. Gallagher, I. T. Rosen, E. J. Fox, L. Jiang, B. Lyu, H. Li, K. Watanabe, T. Taniguchi *et al.*, Nature (London) **572**, 215 (2019).

[2] C. Jin, E. C. Regan, A. Yan, M. Iqbal Bakti Utama, D. Wang, S. Zhao, Y. Qin, S. Yang, Z. Zheng, S. Shi *et al.*, Nature (London) **567**, 76 (2019).

[3] G. Chen, L. Jiang, S. Wu, B. Lyu, H. Li, B. L. Chittari, K. Watanabe, T. Taniguchi, Z. Shi, J. Jung *et al.*, Nat. Phys. **15**, 237 (2019).

[4] B. L. Chittari, G. Chen, Y. Zhang, F. Wang, and J. Jung, Phys. Rev. Lett. **122**, 016401 (2019).

[5] M. Yankowitz, S. Chen, H. Polshyn, Y. Zhang, K. Watanabe, T. Taniguchi, D. Graf, F. Y. Andrea, and R. D. Cory, Science **363**, 1059 (2019).

[6] K. Tran, G. Moody, F. Wu, X. Lu, J. Choi, K. Kim, A. Rai, D. A. Sanchez, J. Quan, A. Singh *et al.*, Nature (London) **567**, 71 (2019).

[7] K. L. Seyler, P. Rivera, H. Yu, N. P. Wilson, E. L. Ray, D. G. Mandrus, J. Yan, W. Yao, and X. Xu, Nature (London) **567**, 66 (2019).

[8] S. Carr, S. Fang, P. Jarillo-Herrero, and E. Kaxiras, Phys. Rev. B **98**, 085144 (2018).

[9] Y. Cao, V. Fatemi, S. Fang, K. Watanabe, T. Taniguchi, E. Kaxiras, and P. Jarillo-Herrero, Nature (London) **556**, 43 (2018).

[10] Y. Cao, V. Fatemi, A. Demir, S. Fang, S. L. Tomarken, J. Y. Luo, J. D. Sanchez-Yamagishi, K. Watanabe, T. Taniguchi, E. Kaxiras *et al.*, Nature (London) **556**, 80 (2018).

[11] J. M. B. Lopes Dos Santos, N. M. R. Peres, and A. H. Castro Neto, Phys. Rev. Lett. **99**, 256802 (2007).

[12] S. Carr, D. Massatt, S. Fang, P. Cazeaux, M. Luskin, and E. Kaxiras, Phys. Rev. B **95**, 075420 (2017).

[13] E. Suárez Morell, J. D. Correa, P. Vargas, M. Pacheco, and Z. Barticevic, Phys. Rev. B **82**, 121407 (2010).

[14] R. Bistritzer and A. H. MacDonald, Proc. Natl. Acad. Sci. USA **108**, 12233 (2011).

[15] G. Trambly de Laissardière, D. Mayou, and L. Magaud, Nano Lett. **10**, 804 (2010).

[16] C. Kane, L. Balents, and M. P. A. Fisher, Phys. Rev. Lett. **79**, 5086 (1997).

[17] R. Egger and A. O. Gogolin, Phys. Rev. Lett. **79**, 5082 (1997).
[18] M. Bockrath, D. H. Cobden, J. Lu, A. G. Rinzler, R. E. Smalley, L. Balents, and P. L. McEuen, Nature (London) **397**, 598 (1999).
[19] H. Ishii, H. Kataura, H. Shiozawa, H. Yoshioka, H. Otsubo, Y. Takayama, T. Miyahara, S. Suzuki, Y. Achiba, M. Nakatake *et al.*, Nature (London) **426**, 540 (2003).
[20] Z. Shi, X. Hong, H. A. Bechtel, B. Zeng, M. C. Martin, K. Watanabe, T. Taniguchi, Y.-R. Shen, and F. Wang, Nat. Photon. **9**, 515 (2015).
[21] S. Zhao, R. Kitaura, P. Moon, M. Koshino, and F. Wang, Adv. Sci. **9**, 2103460 (2022).
[22] M. Koshino, P. Moon, and Y.-W. Son, Phys. Rev. B **91**, 035405 (2015).
[23] X. Zhou, J. Xie, G. Li, J. Zhang, M. Xia, W. Luo, and Z. Shi, Phys. Rev. B **105**, 115433 (2022).
[24] Q. Gao, J. Chen, B. Lyu, A. Deng, L. Wang, T. Wu, K. Watanabe, T. Taniguchi, and Z. Shi, Appl. Phys. Lett. **117**, 023101 (2020).
[25] N. A. Lanzillo, N. Kharche, and S. K. Nayak, Sci. Rep. **4**, 3609 (2014).
[26] O. Arroyo-Gascón, R. Fernández-Perea, E. Suárez Morell, C. Cabrillo, and L. Chico, Nano Lett. **20**, 7588 (2020).
[27] O. Arroyo-Gascón, R. Fernández-Perea, E. S. Morell, C. Cabrillo, and L. Chico, Carbon **205**, 394 (2023).
[28] C. Chen, Y. Lin, W. Zhou, M. Gong, Z. He, F. Shi, X. Li, J. Z. Wu, K. T. Lam, J. N. Wang *et al.*, Nat. Electron. **4**, 653 (2021).
[29] P. E. Lammert, P. Zhang, and V. H. Crespi, Phys. Rev. Lett. **84**, 2453 (2000).
[30] J. Q. Lu, J. Wu, W. Duan, F. Liu, B. F. Zhu, and B. L. Gu, Phys. Rev. Lett. **90**, 156601 (2003).
[31] M. Yankowitz, J. Jung, E. Laksono, N. Leconte, B. L. Chittari, K. Watanabe, T. Taniguchi, S. Adam, D. Graf, and C. R. Dean, Nature (London) **557**, 404 (2018).
[32] N. Morales-Durán, J. Wang, G. R. Schleder, M. Angeli, Z. Zhu, E. Kaxiras, C. Repellin, and J. Cano, Phys. Rev. Res. **5**, L032022 (2023).
[33] L. G. Pimenta Martins, D. A. Ruiz-Tijerina, C. A. Occhialini, J.-H. Park, Q. Song, A.-Y. Lu, P. Venezuela, L. G. Cançado, M. S. C. Mazzoni, M. J. S. Matos *et al.*, Nat. Nanotechnol. **18**, 1147 (2023).
[34] T. Ando, J. Phys. Soc. Jpn. **74**, 777 (2005).
[35] C. Zhang, K. Bets, S. S. Lee, Z. Sun, F. Mirri, V. L. Colvin, B. I. Yakobson, J. M. Tour, and R. H. Hauge, ACS Nano **6**, 6023 (2012).
[36] M. He, J. Dong, K. Zhang, F. Ding, H. Jiang, A. Loiseau, J. Lehtonen, and E. I. Kauppinen, ACS Nano **8**, 9657 (2014).
[37] N. G. Chopra, L. X. Benedict, V. H. Crespi, M. L. Cohen, S. G. Louie, and A. Zettl, Nature (London) **377**, 135 (1995).
[38] A. P. Thompson, H. M. Aktulga, R. Berger, D. S. Bolintineanu, W. M. Brown, P. S. Crozier, P. J. in 't Veld, A. Kohlmeyer, S. G. Moore, T. D. Nguyen *et al.*, Comput. Phys. Commun. **271**, 108171 (2022).
[39] S. J. Stuart, A. B. Tutein, and J. A. Harrison, J. Chem. Phys. **112**, 6472 (2000).
[40] P. Moon and M. Koshino, Phys. Rev. B **90**, 155406 (2014).
[41] F. Munoz, H. P. O. Collado, G. Usaj, J. O. Sofo, and C. A. Balseiro, Phys. Rev. B **93**, 235443 (2016).
[42] See Supplemental Material at http://link.aps.org/supplemental/10.1103/PhysRevB.109.045105 for more details.
[43] J. Zaanen, G. A. Sawatzky, and J. W. Allen, Phys. Rev. Lett. **55**, 418 (1985).
[44] Y. Zhang, N. F. Q. Yuan, and L. Fu, Phys. Rev. B **102**, 201115(R) (2020).
[45] B. A. Foutty, J. Yu, T. Devakul, C. R. Kometter, Y. Zhang, K. Watanabe, T. Taniguchi, L. Fu, and B. E. Feldman, Nat. Mater. **22**, 731 (2023).